Performance Evaluation of Alumina-graphene Hybrid Nano-cutting Fluid in Hard Turning of AISI 304 Steel

Abstract

Nanofluid (NF) is a colloidal mixture of metallic or non-metallic particles of nanometre-size in a base fluid. In the present investigation, a hybrid nano-cutting fluid with better thermal and tribological properties has been developed by mixing alumina based nanofluid with graphene nanoplatelets (GnP) in the volumetric concentrations of 0.25, 0.75 and 1.25 vol. %. The prepared hybrid and alumina mixed nanofluids are characterized for their thermal conductivity, viscosity, specific heat and density in various nanoparticle concentrations at different temperatures. Furthermore, pin on disc testing and contact angle measurement of all nanofluid samples are performed to understand their tribological behaviour and wettability, respectively. Later the performance of the prepared cutting fluid was evaluated during turning of AISI 304 steel under minimum quantity lubrication (MQL) technique. The results have also been compared with the results obtained with that of alumina nanofluid. The results clearly establish that the performance of hybrid nanofluid, in terms of cutting force, feed force, thrust force and surface roughness, is significantly better as compared to alumina nanoparticle mixed cutting fluid.

Keywords*:* Hybrid; nanofluid; MQL; Graphene; Roughness; Force; Turning

1. Introduction

In the manufacturing industry, during dry machining of steel, due to high degree of heat generation at the machining zone, cutting velocity of the tool gets restricted. Moreover, the heat affects hardness and sharpness of the cutting tools and result in their premature breakage. Therefore, a suitable cutting fluid becomes necessary in order to overcome these difficulties in high speed machining. Cutting fluid plays a vital role by cooling and lubricating the cutting tool work piece interface and washing away the chips from machining zone. This conventional way of cooling, however, serves the purpose up to an extent. Excessive use of the conventional cutting fluids pollutes the environment and may even be hazardous for human beings.

To restrict excessive use of conventional cutting fluids, MQL/NDM (near dry machining) has emerged as a promising technique. In this technique, a small quantity of any cutting fluid has to be sprayed into the cutting zone at high pressure so that it can penetrate the machining zone properly. Cetin et al. (2011) found that the MQL technique is capable of spraying cutting fluid into the cutting zone optimally. Hadad and sadeghi (2013) noticed that the best surface quality could be achieved over entire range of depth of cut by using the MQL technique in turning of 4140 alloy steel. A few researchers like Sharma et al. (2016) and Sarikya and Gullu (2015) concluded that the use of the MQL technique improves the surface finish, tool life and reduces impact of the cutting forces. In their opinion, it can be a viable alternative to wet machining because the MQL technique can minimize both, the manufacturing cost and the environmental hazards.

Conventional fluids may possess good lubrication properties but poor thermal properties in them restrict their use as cutting fluid for industrial purpose. By mixing milli or micro-sized solid particles, thermal conductivity (heat extraction capability) of conventional fluids may be increased. However, use of micro-sized particles may create serious problems of clogging and pressure drop in pipelines. They also have poor stability of suspension. To overcome these problems, nanometre-sized particles have replaced micro particles, leading to the synthesis of a new generation fluids, which are called 'nanofluids'. The use of these nanofluids has shown a noticeably improved performance in different machining processes.

Tiwari et al. (2012) reported a significant improvement in thermal conductivity of conventional fluid (water) by the inclusion of different nanoparticles and noticed a further enhancement with a rise of nanoparticle volumetric concentration in the base fluid. Few researchers like Yang (2006) and Choi et al. (2001) noticed a massive increment of approx. 200% and 150% respectively in thermal conductivity when multi-walled carbon nanotube (MWCNT) was added to the base fluid. Moreover, Sharma et al. (2015a) reviewed various published research works on nano-cutting fluid and found that mixing of nanoparticles into cutting fluid enhances its thermal conductivity, which in turn, improves the tool life and reduces the cutting force, surface roughness and cutting temperature.

Besides thermal conductivity of cutting fluid, the friction between cutting tool and work piece interface plays a critical role in heat generation at machining zone. It increases the tool tip temperature, and, in turn, may also decrease hardness and sharpness of the tool cutting edge. As a result, the surface finish gets affected and the tool wear is aggravated. Sharma et al. (2015b) investigated the performance of the multi walled carbon nanotube (MWCNT) enriched cutting fluid in turning of AISI D2 steel and noticed an appreciable reduction in tool temperature and surface roughness. It has been found that addition of graphite nanoparticles into the base fluid enhances its tribological property due to reduced coefficient of friction (Lee et al., 2009). Due to their low friction behaviour, MoS_2 and graphite solid lubricants reduce surface roughness and cutting force during machining (Reddy and Rao, 2006). They also ensure an improved surface quality and a reduction in tool wear, cutting force and chip thickness compared to dry and conventional wet machining (Khandekar et al., 2012). Park et al. (2011) investigated the effect of graphene nanoplatelets enriched vegetable oil in milling operation. They observed an improved wettability and reduced friction at the machining zone which in turn reduced the tool wear and yielded better machining performance. Sayuti et al. (2014) examined the novel use of SiO_2 nanoparticle enriched cutting fluid in hard turning and observed less cutting fluid consumption with better surface quality and tool wear. Albert et al. (2009) used graphene enriched mineral oil in grinding and achieved a significant reduction in surface roughness, grinding forces and specific energy consumption. Moreover, Amrita et al. (2014) evaluated the performance of nano-graphite based nano cutting fluid in turning and found that MQL method reduces the surface roughness, cutting force, cutting temperature and tool wear by 30%, 54%, 25% and 71%, respectively, in comparison with the conventional wet machining.

The exhaustive literature review by Sharma et al. (2015a) reveals a lot of work being carried out in the field of conventional machining with nano-cutting fluids enriched with a single type of nanoparticles. However, to the best of author's knowledge, very few investigations have been performed with the use of hybrid nanofluids (i.e. a colloidal suspension enriched by two different types of nanoparticles). Moreover, Sarkar et al. (2015) reviewed the available literature on hybrid nanofluids and concluded that the proper hybridization might be helpful in making hybrid nanofluids very auspicious for heat transfer enhancement. Zhang et al. (2016) in their investigation on lubrication performance of Al_2O_3-SiC enriched nanofluid during MQL grinding of Ni-based alloy opined that the Al_2O_3-SiC enriched nanofluid yielded better surface quality compared with pure nanoparticles. Furthermore, Ahammed et al. (2016) recorded an enhancement of 88.62% in convective heat transfer coefficient and a reduction of 4.7 °C in equipment temperature by the use of alumina-graphene hybrid nanofluid. Zhang et al. (2015) used MoS_2-CNT hybrid nanofluid in grinding operation and observed that for the same mass fraction, MoS_2-CNTs hybrid nanofluid achieved lower G ratio and surface roughness ($R_a = 0.328$ μm) compared with pure MoS_2 and CNT nanoparticles. This may be attributed to the physical collaboration of the mixed nanoparticles. Many researchers have also performed the thermos-physical characterization of hybrid nanofluids and found that hybridization of different types of nanoparticles may enhance the thermos-physical (Abbasi et al., 2013) and tribological (Kanthavel et al., 2016) properties of base nanofluid. However not much significant work could be reported in literature regarding the application of hybrid nanofluids as a cutting fluid in machining, especially in turning operation.

In present work, a hybrid nano-cutting fluid has been developed by mixing graphene nanoplatelets with alumina based nanofluid in different volumetric concentrations of 0.25, 0.75 and 1.25 vol. %. All the nanofluid samples have been tested for their thermal conductivity and viscosity at different temperatures in different concentrations followed by the study of their wettability in terms of contact angle and tribological behaviour on pin on disc testing machine. At last, their performances as a cutting fluid has been evaluated in turning of AISI 304 steel regarding three components of machining forces (cutting, thrust, and feed force) and surface roughness by using minimum quantity lubrication (MQL) technique. The results are also compared with the performance of alumina nanoparticle mixed cutting fluid.

2. Experimental Procedure

Prior to the application of nanofluids in machining, the samples were tested for thermo-physical properties such as thermal conductivity and viscosity followed by their tribological testing and wettability study.

2.1 Preparation and characterization of nanofluids

The commercially available colloidal suspension containing 25 vol.% of Al_2O_3 nanoparticles (spherical in shape with 45 nm in diameter) in water, was procured from Alfa Aesar® and water based colloidal suspension containing 18 vol.% of graphene (average thickness: 11-15nm, average particle size: 5 microns) was purchased from Sigma Aldrich. The surfactant CTAB was already added to the suspension by the manufacturer. The alumina-graphene (Al-GnP) hybrid nanofluid

was prepared by mixing Al_2O_3 with graphene nanoplatelets (GnP) in volumetric ratio of 90:10 in the same base fluid in three volumetric concentrations (0.25%, 0.75% and 1.25% vol.). The base fluid was prepared by mixing 5 vol. % vegetable oil in deionized water. The detergent in volumetric proportion of 0.5 % was used as an emulsifier to get stable emulsion (base fluid). The TEM images shown in Fig. 1 justify the size of nanoparticles present in colloidal suspension.

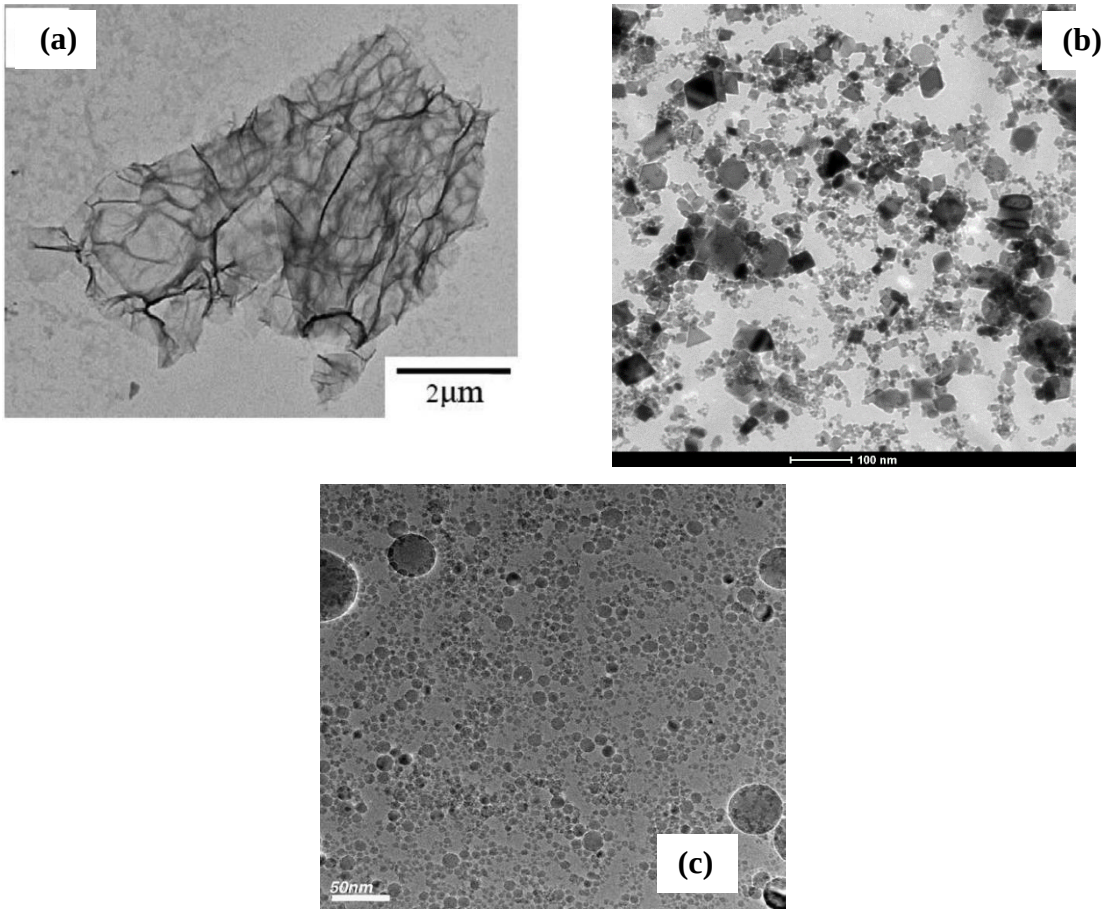

Fig.1 TEM images of (a) GnP (b) Alumina nanofluid and (c) Al-GnP hybrid nanofluid

The prepared nano fluids were kept in ultrasonicator (Toshiba, India), generating 100W ultrasonic pulses at 36±3 kHz at a stretch for 6 hours to get a homogeneous and stable suspension. A fresh nano-cutting fluid sample was developed for each test and used immediately to avoid possible agglomeration/sedimentation. The prepared hybrid nanofluids were tested for thermo physical properties (thermal conductivity and viscosity) at five temperatures: 25, 35, 40, 45 and 50 °C. The effect of nanoparticle concentration on its properties was also studied. A transient hot wire apparatus (Decagon Devices, Inc., USA) was used to determine nanofluids' thermal conductivity. The hot-wire measures the thermal conductivity and thermal resistivity from the rate of rise in temperature of the probe for constant rate of heating. The viscosity of various nanofluids was

measured with the help of digital viscometer equipped with a temperature bath which sets the temperature of nanofluid at different values.

The Al-GnP hybrid nanofluid shows an improvement in thermal conductivity over base fluid while surprisingly, the hybridization of alumina with GnP reduced its (hybrid nanofluid) thermal conductivity compared to pure alumina nanofluid. An enhancement of 9.38% in thermal conductivity could be observed by the blending of graphene, however alumina alone has shown an improvement of 9.85%, even better than Al-GnP hybrid nanofluids as illustrated in Fig 2.

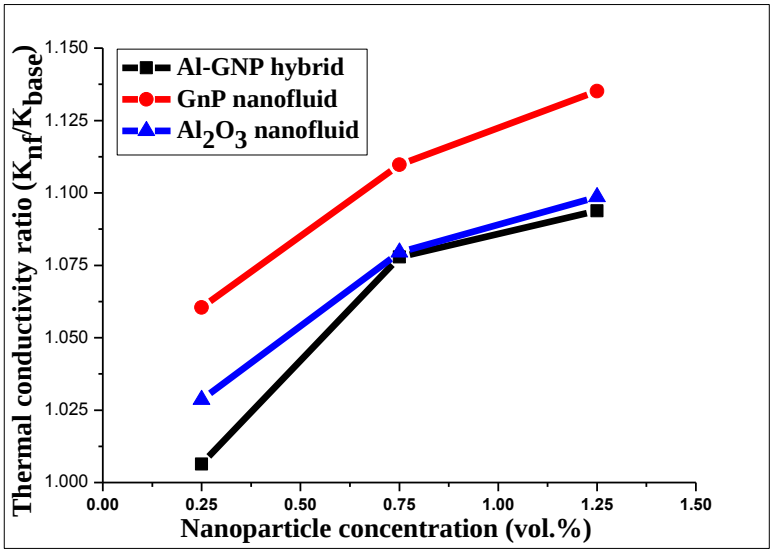

Fig. 2 Thermal conductivity ratio of nanofluids at different nanoparticle concentrations

All the hybrid nanofluids samples have shown a reduction in viscosity with increase of temperature. Fig. 3 clearly shows an increment of 17.69%, 25.19%, and 31.53% in viscosity of Al-GnP hybrid nanofluid for concentration of 0.25%, 0.75% and 1.25%, respectively. Further it is found that all the nanofluids show a reduction in viscosity with rise of temperature largely following the behaviour of pure water for small particle content.

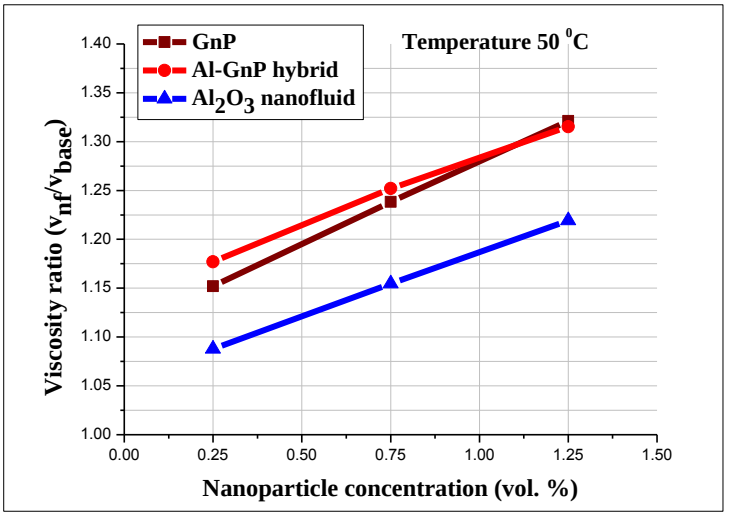

Fig. 3 Viscosity ratio of different nanofluids at different nanoparticle concentrations

This observation clearly reveals that an increase of nanoparticle concentration enhances both, the thermal conductivity and viscosity. Thermal conductivity positively affects the cooling of the tool-work piece interface while higher viscosity creates problem (pressure drop due to high viscosity) while spraying nano-cutting fluid with the MQL technique. In order to balance the benefit of higher thermal conductivity and the loss of pumping power due to high viscosity, the authors selected a volumetric range of 0.25 vol. % to 1.25 vol. % for further experimental investigation. Later, all the nanofluids samples were kept on ultrasonic vibrator for about two hours to get a homogeneous and stable nanofluid. As a result, during further tribological study, wettability testing and turning operation, no precipitation of nanoparticles was noticed. Furthermore, nanofluids' specific heat and density variation were measured.

2.2 Tribology testing of nanofluids

The determination of experimental value of coefficient of friction in turning operation is a tidious task. Therfore, to understand the tribological behaviour of nanofluids, a series of experiments were performed on a pin on disc wear and friction tester TR-20 (Ducom, India) with maximum speed and load capacity of 2000 RPM and 1000 N, respectively. The complete experimental setup is illustrated in Fig 4. Cylindrical pin (Dia. 3 mm, length 40 mm) and disc (pitch circle dia. 155 mm) made up of AISI 304 steel were used in this experiment. During the experiments, the load, linear speed and time were kept constant at 40 N, 1 m/s and 5 min, respectively. The sliding track of pin was changed after each run to ensure the availability of fresh surface to next run and to maintain the constant sliding speed, RPM of the disc were changed

accordingly. The steel disc was cleaned with acetone after each run to ensure smooth and clean disc surface.

Fig 4 (a) Pin-on-disc experimental setup (b) Pin and Disc machine (c) closed view of sliding pin on rotating disc

The different samples of Al_2O_3 nanofluid, Al-GnP hybrid nanofluid in three volumetric concentrations (0.25, 0.75 and 1.25 vol. %) and base fluid (5 vol. % oil-water emulsion) were used as a lubricant during the wear testing. The wear of steel pin as a function of nanoparticle concentration for different lubricating conditions is depicted in Fig 5(a). A reduction in wear was observed with an increase of nanoparticle concentration for monotype and hybrid nanofluid. This may be attributed to the formation of a nano-layer between the sliding surfaces of pin and disc, and intensity of layer could be enhanced by the presence of more number of nanoparticles at higher concentrations. Moreover, a higher rate of wear was observed initially, and after some time the wear rate stabilises for all the samples (Fig 5(b)). It can be seen from Fig 5(c) that Al-GnP hybrid nanofluid exhibits the highest lubricating property followed by monotype alumina nanofluid. Alumina nanofluid and base fluid produced comparable results, but significantly better than dry condition.

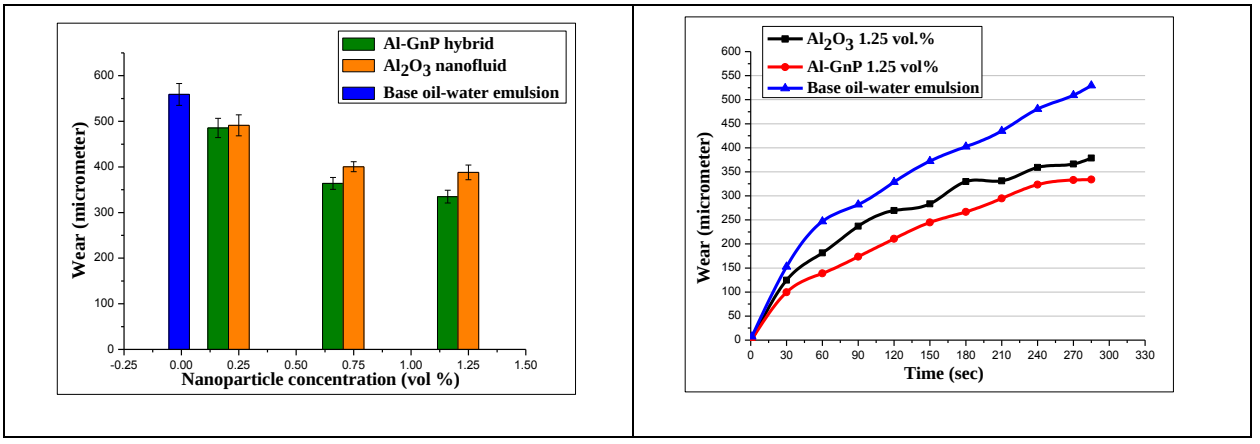

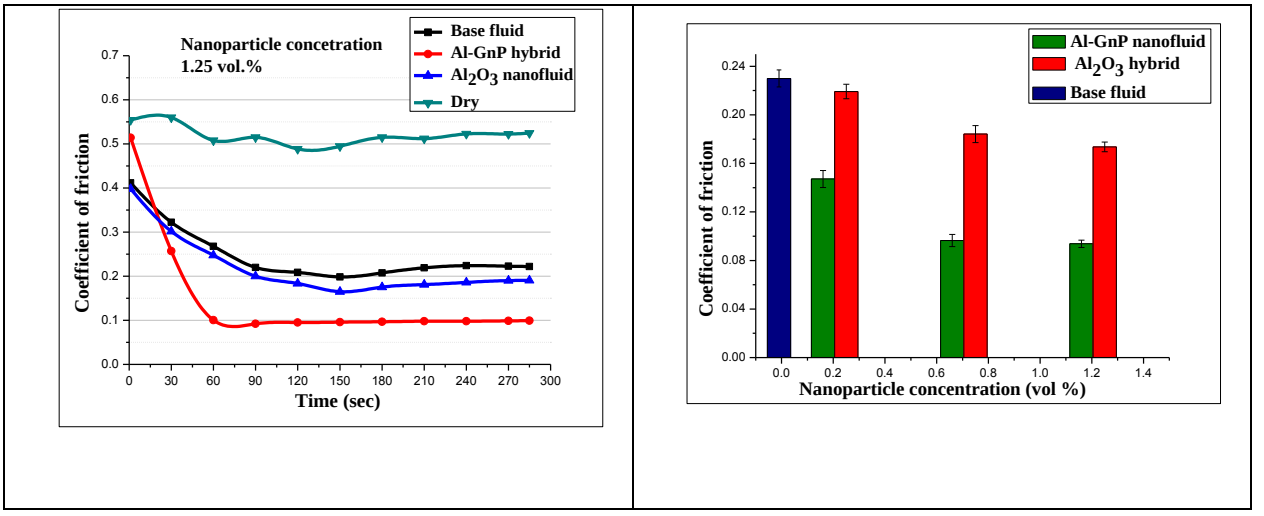

Fig 5 Wear of AISI 304 pin as a function of (a) nanoparticle concentration (b) time for different lubricating mediums (c) Coefficient of friction for different lubricating mediums w.r.t. time (d) w.r.t. nanoparticle concentration

Fig 5(d) depicts that Al-GnP hybrid nanofluid possesses the lowest coefficient of friction for all volumetric concentrations followed by monotype alumina nanofluids. As earlier stated, this may be attributed due to the formation of a nano-layer between the sliding surfaces of pin and disc. Furthermore, this reducing trend of the coefficient of friction with an increase in nanoparticle concentration has shown a reduction in the friction force.

Fig 6 presents the FESEM images of the sliding surface of the pin during the pin-on-disc experiment for various lubricating mediums at a magnification of 100X and 1.00KX. A noticeable qualitative difference in the surface morphology could be seen. Moreover, it can easily be noticed that best surface quality is seen in the case of Al-GnP hybrid nanofluid and manifested as a superior lubricating medium over monotype alumina nanofluid and base fluid.

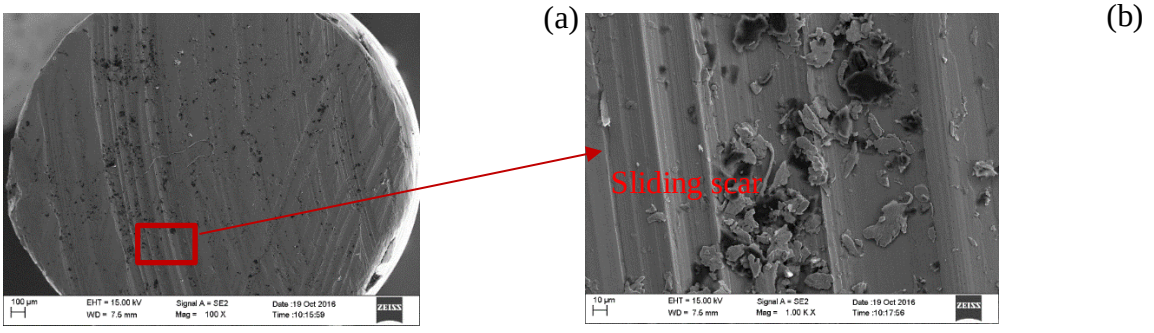

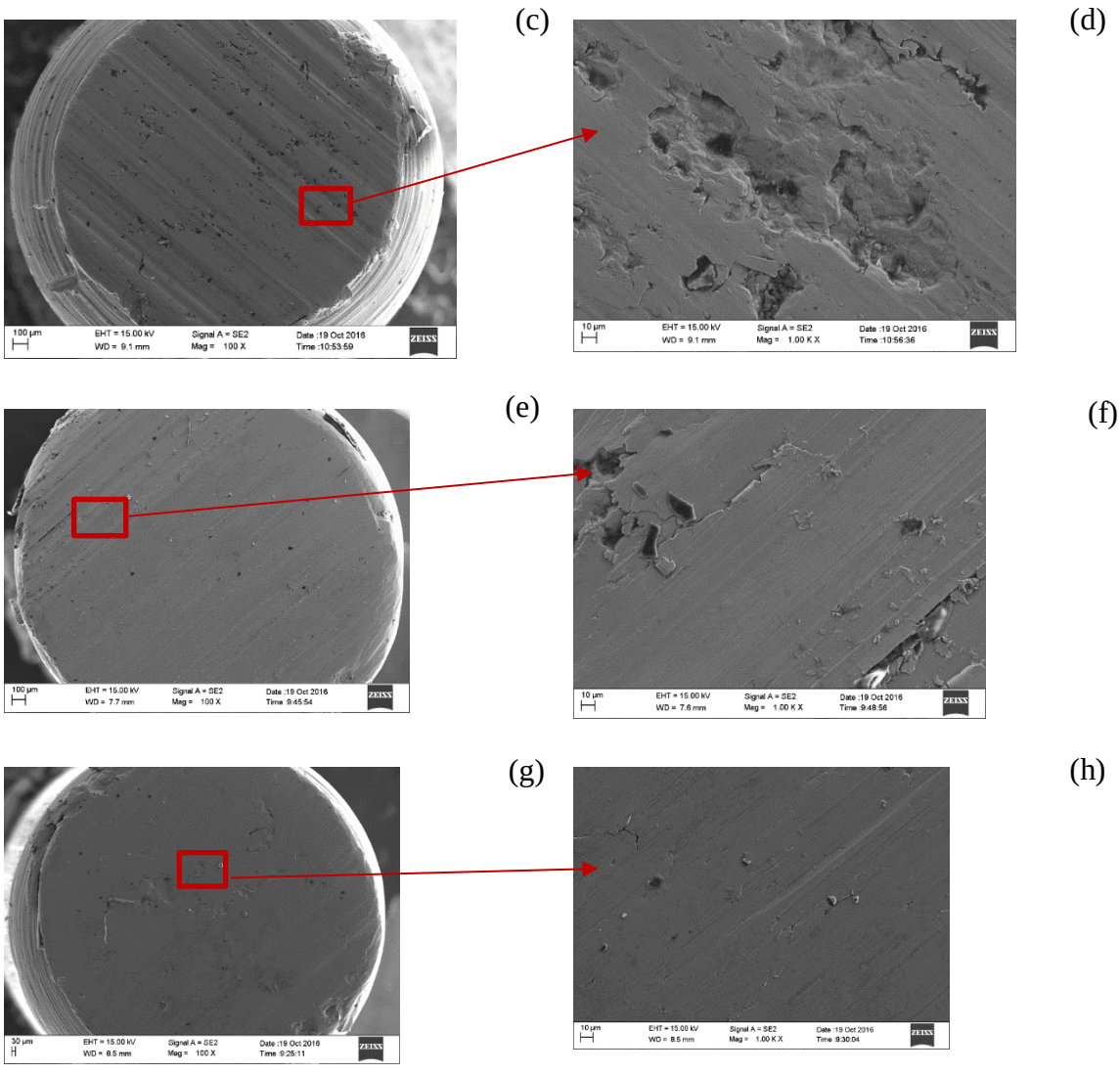

Fig 6 FESEM images of pin wear under (a-b) dry (c-d) base fluid (e-f) Al_2O_3 (g-h) Al-GNP nanofluids in pin-on-disc test

2.3 Contact angle measurement for nano-cutting fluids

Spreadability of cutting fluid over tool surface may enhance the heat extraction from hot tool surface. The wettability characteristics of any cutting fluid can be determined by the measurement of the contact angle between the solid surface and the droplet.

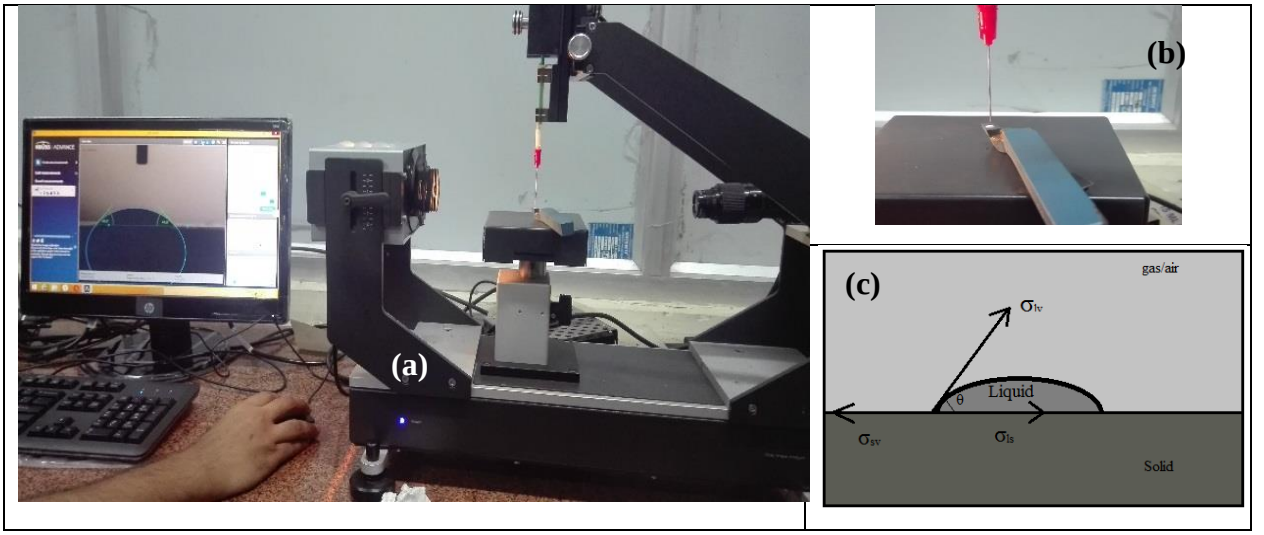

Fig 7 (a) Contact angle measurement setup (b) closed view of dropper and carbide tool (c) Schematic diagram showing a liquid droplet on solid surface

The determination of contact angle is often based on Young's (1805) contact angle equation (Eq. 1). This equation explains an equilibrium force balance at three phase (air as the third phase) interface illustrated in Fig 7(c) (Khandekar et al., 2012). The equilibrium thermodynamic contact angle is given by:

$$\cos\theta = \frac{\sigma_{sv} - \sigma_{sl}}{\sigma_{lv}} \qquad (1)$$

Where θ is equilibrium contact angle, σ_{lv}, σ_{sv} and σ_{sl} are liquid-vapour, solid-vapour, and solid-liquid interfacial tensions, respectively.

The free energy of a system depends on the intermolecular force potentials of constituent molecules/atoms which give rise to surface tension phenomenon. Also, the net surface tension of any liquid strongly depends on Van der Walls forces (Khandekar et al., 2012). These forces have interaction length scale of nanometre size, equivalent to that of nanoparticle size. So it is expected that addition of nanoparticles affects the net free energy of a pure liquid-solid-air interface. For testing this hypothesis, the spreadability of all nanofluids (nanofluids of different nanoparticle concentrations i.e. 0%, 0.25%, 0.5%, 0.75%, 1.0 %, 1.25% and 1.5 %) was determined by the measurement of the macroscopic contact angle between the fluid droplet and cemented carbide tool insert surface. The contact angle measurement setup is illustrated in Fig 7. The measurement of contact angle (θ) was performed by using a drop shape analyzer 25 (KRUSS), with an inbuilt software DSA 4. The cutting tool (carbide insert) surface was kept in the environment chamber at

room temperature. The chamber was allowed to come to equilibrium conditions so that a saturated relative humidity environment was established. Then, accurately measured 10 µl cutting fluid was carefully dropped through the 0.5 mm OD needle tip on the top surface of the surface. The camera of the instrument was perfectly adjusted to take the drop image formed on the tool surface and contact angle data was measured by the inbuilt software.

Fig 8 clearly shows that wettability (contact angle) of nano-cutting fluid is affected significantly by the addition of nanoparticles. As nanoparticle concentration increases from 0% to 1.5 %, the contact angle first reduces and then it increases for higher concentrations for all nanofluids samples. This can be justified by the findings of Wasan et al. (2011) who noticed an increase in contact diameter (spreading of the droplet) with an increase of nanoparticle concentration in the conventional fluid. The smallest contact angle for Al-GnP and alumina nanofluids could be recorded as 38.9º (at 1.0 vol%) and 41.9º (at 1.0 vol%), respectively, thus, gave maximum wetting area per unit liquid volume. The contact angle for base fluid was recorded as 54.9º, which is much higher as compared to the contact angle measured for each nanofluid. So it improves the heat extraction and lubricating properties compared to base fluid. The findings are in good agreement with the results obtained in previous investigations (Khandekar et al., 2012, Park et al., 2011)).

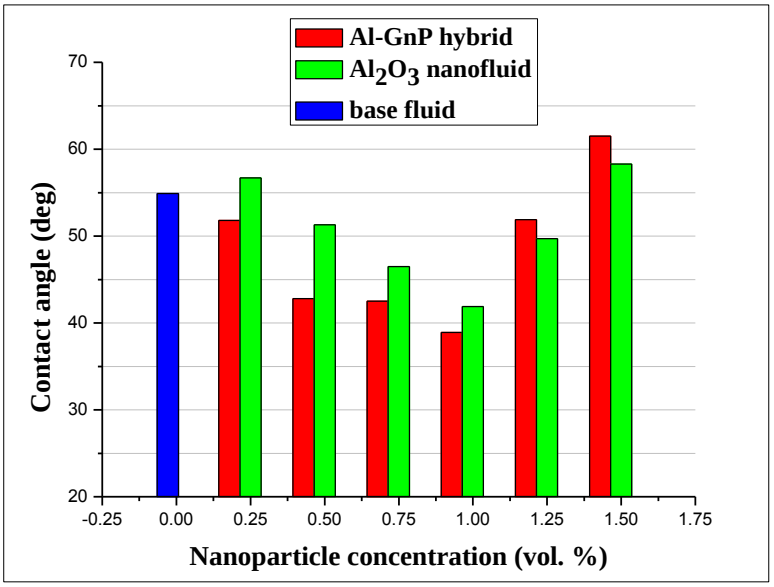

Fig 8 Contact angle as a function of nanoparticle concentration of different nanofluids

2.4 Experimental setup

Turning of AISI 304 steel was carried out on HMT (model NH 22/1500) lathe machine under mist of different nanofluids using MQL technique. The pictorial view of experiment setup is shown in Fig 9. The coated cemented carbide insert (Widia's CCMT 09T304-TN2000) was mechanically clamped on a rigid tool holder (widax SCLCR1212F09 D 3J). The MQL system involves a compressor, a flow controlling unit, an air-dryer and a spray nozzle. The nanofluid flow rate and air supply pressure for MQL system are set at 2.5 ml/min and 4 bar, respectively. A discharge nozzle is placed at a distance of 5 cm just above the rake face of cutting tool, capable of impinging mist vertically downward on tool (Fig. 9(b)). As a result, the mist of nano-cutting fluid effectively falls in the cutting zone.

(a)

1. HMT Lathe (NH22) machine
2. Microprocessor based speed controller
3. Spray nozzle
4. Kistler force dynamometer
5. Kistler charge amplifier
6. Force display unit
7. MQL unit
8. Air dryer
9. Air compressor
10. Carbide cutting insert

Fig 9(a) Pictorial view of experimental setup (b) closed view of machining zone

All the experiments were conducted in triplicate and the average of the values was considered. Cutting forces were calculated by using three-component piezoelectric Kistler dynamometer (Type 9047CNK). For analysis, mean values of the cutting forces were noted over a regular interval of time. The average surface roughness (R_a) of the work piece was measured by Surftest SJ-210 (Mitutoya make) after every turning operation under different machining environments. This

exercise was repeated at six reference points at 60° angle on the cylindrical surface of the work piece. Surftest SJ-210 is a contact-type measuring instrument with a probe (having diamond tip of 2µm-radius) that is able to travel on the work piece surface. The instrument has a measuring range of 360 µm (-200 µm to 160 µm), measuring speed of 0.25 mm/sec, probe returning speed of 1 mm/sec and cut off length of 0.08 mm.

2.5 Experimental design using Response surface methodology

Response Surface Methodology (RSM) is a collection of statistical techniques that are useful for the modeling and analysis of problems in which one or more responses of interest are influenced by several variables and has two objectives: first is to find the relationship between responses and several variables and second to optimize the responses. The first step in RSM is to find a suitable approximation for the true functional relationship between response y and a set of independent variables employed. When the independent variables change values in certain directions, the responses should also change (Montgomery, 2009). In other words, RSM tends to focus on the relationships between multiple factors (x_1, x_2, x_3, ..., x_k) and the response (y). Consequently, the functional relationship between the responses and the independent variables should first be determined to produce a proper approximating function, and then the factor setting levels needed to obtain the optimal response should be identified. The relationship between the response variables and the independent variables (factors) can be presented in the form of the following equation.

$$y = f(x_1, x_2, x_3, \dots\dots\dots\dots x_k)$$

Where f is a multivariate function, the items represent the factors (independent variables), and the relationship describes a curved surface $y = f(x_1, x_2, x_3 \dots\dots, x_k)$ that is known as a Response Surface.

Usually, a second order model is utilized in RSM (Gopal and Rao, 2003). A second-order model can significantly improve the optimization process when a first-order model suffers a lack of fit due to the interaction between variables and surface curvature. A general second-order model is defined as

$$y = a_o + \sum_{i=1}^{n} a_i x_i + \sum_{i=1}^{n} a_{ii} x_i^2 + \sum_{i=1}^{n} \sum_{j=1}^{n} a_{ij} x_i x_j \qquad : i<j$$

Where, a_0 is the constant and a_i, a_{ii} and a_{ij} are respectively, the coefficients of first-order (linear), second-order (quadratic) and cross-product terms. The term x_i and x_j represent the input variables.

The input variables were optimized by RSM, using a Box-Behnken design to get the optimized value of response parameters. Box-Behnken design has three levels (low, medium, and high, coded as -1, 0, and +1) and needs fewer experimental runs and less time. A total number of 27 trials including three center points were employed. All the experiments were performed independently in triplicates, and the average values were presented as the response. The process variable (input machining parameters) with their values on different levels are listed in Table 1. The Design Expert 10.0 was applied for the Box-Behnken experimental design, regression analysis of the experimental data, quadratic model buildings and also to plot three-dimensional response surface plots. Statistical analysis of the models was used to evaluate the analysis of variance (ANOVA). The quality of fit the second-order polynomial model equation was judged statistically via the coefficient of determination R^2 and the adjusted R^2. The fitted polynomial equation was then expressed regarding three-dimensional surface plots to evaluate the relationship between the responses and visualize the interaction between the variables utilized in the study. The point optimization method was conducted to optimize the level of each variable for a desirable response. The combination of different optimized input variables, which yielded the desired value of the response, was determined in an attempt to verify the validity of the model. At last, validation experiments were performed to check the adequacy of the experimental setup.

Table 1 Control factors and their levels

Control factor	**Symbol**	**Units**	**Level 1**	**Level 2**	**Level 3**
Cutting speed	V	m/min	60	90	120
Cutting feed	F	mm/rev	0.08	0.12	0.16
Depth of cut	D	mm	0.6	0.9	1.2
Nanoparticle concentration	Np	vol %	0.25	0.75	1.25

Table 2 summarizes the design of experiment with experimental run order and output in the terms of four response parameters for alumina based nanofluid and Al-GnP hybrid nanofluid.

Table 2 Machining variables and response parameters

Run	Input Machining parameters				Response variables							
					Alumina nanofluid				Al-GnP hybrid nanofluid			
	V (m/min)	f (mm/rev)	d (mm)	np (vol.%)	F_z (N)	F_y (N)	F_x (N)	R_a (μm)	F_z (N)	F_y (N)	F_x (N)	R_a (μm)
1	90	0.16	1.2	0.75	527.275	287.955	103.296	2.712	481.425	259.965	98.1	2.169
2	60	0.12	1.2	0.75	475.335	259.26	94.389	2.367	434	234.128	88.35	1.893
3	120	0.12	0.9	1.25	314.111	240.305	76.872	1.474	340.673	241.76	91.23	1.179
4	60	0.12	0.6	0.75	256.83	181.665	56.955	2.234	217	164.009	61.89	1.787
5	90	0.12	0.9	0.75	361.039	222.605	74.799	1.978	329.647	200.976	75.84	1.582
6	60	0.12	0.9	0.25	444.668	243.62	89.136	2.456	406	238.023	89.82	1.995
7	120	0.12	1.2	0.75	479.339	292.275	95.082	1.823	317.24	263.861	99.57	1.458
8	120	0.08	0.9	0.75	241.584	217.98	54.363	1.568	236.67	196.286	74.07	1.435
9	90	0.08	1.2	0.75	350.378	218.465	72.969	1.656	311.346	197.239	74.43	1.325
10	60	0.08	0.9	0.75	260.687	174.92	62.802	1.824	242.55	157.887	59.58	1.459
11	90	0.12	0.9	0.75	347.774	217.415	72.525	1.945	317.52	196.286	74.07	1.556
12	120	0.12	0.9	0.25	395.178	221.66	82.032	1.856	340.97	200.101	75.51	1.548
13	90	0.12	1.2	1.25	464.884	247.205	92.619	1.901	424.462	232.22	87.63	1.220
14	90	0.12	0.9	0.75	381.591	230.725	78.462	1.911	348.39	208.29	78.6	1.528
15	60	0.16	0.9	0.75	441.945	254.43	88.659	2.973	403.515	215.604	81.36	2.378
16	120	0.12	0.6	0.75	173.075	148.785	42.576	1.899	158.025	134.275	50.67	1.652
17	90	0.12	0.6	0.25	218.995	166.87	50.439	2.034	199.92	150.653	56.85	1.627
18	90	0.08	0.6	0.75	138.866	95.415	36.702	1.611	126.787	86.0985	32.49	1.288
19	90	0.08	0.9	0.25	297.045	197.475	63.825	2.197	271.215	178.319	67.29	1.757
20	90	0.08	0.9	1.25	253.575	180.415	56.388	1.527	231.525	162.896	61.47	1.222
21	60	0.12	0.9	1.25	335.685	195.16	69.441	2.116	306.495	191.993	72.45	1.692
22	90	0.12	1.2	0.25	484.204	271.07	95.919	2.111	442.103	244.701	92.34	1.689
23	90	0.12	0.6	1.25	199.234	159.06	47.046	1.899	181.912	127.677	48.18	1.419
24	90	0.16	0.6	0.75	236.684	173.775	53.469	2.656	216.09	156.854	59.19	2.125
25	90	0.16	0.9	1.25	412.965	243.08	83.775	2.455	377.055	219.42	82.8	1.764
26	90	0.16	0.9	0.25	449.211	257.27	89.922	2.745	410.13	232.299	87.66	2.196
27	120	0.16	0.9	0.75	435.785	276.065	84.102	2.499	397.72	245.718	92.95	1.849

3. Results and discussion

3.1 Machining with alumina nanoparticle mixed cutting fluid

The variance analysis of response parameters was made with the objective of analysing the influence of nanoparticle inclusion on the obtained results. Table 3-6 show the results of ANOVA, respectively for F_z, F_y, F_x, and R_a. This analysis was carried out at a confidence level of 95% (i.e. 5% significance level). The last column of these tables show the influence of variation in input variables (significant or non-significant) on response parameter (output). Table 3 shows that V, f, d and np all have significant effect on the cutting force. It can be depicted from Tables 4-5 that np

and its interaction with speed have a significant effect on thrust force and feed force. Table 6 clearly reveals that feed is the most significant factor associated with surface roughness, because its increase generates helicoids and these helicoids become broader and deeper with the increase of feed rate. Similar findings were observed by Bouacha et al. (2010) in their investigations.

Table 3 ANOVA table of cutting force (F_z) for Al_2O_3 nanofluid

Source	Sum of Squares	DF	Mean Square	F-value	Prob.
Model	301500	14	21538.93	45.32	< 0.0001
A-V	2583.62	1	2583.62	5.44	0.0380
B-f	77077.05	1	77077.05	162.16	< 0.0001
C-d	202200	1	202200	425.43	< 0.0001
D-np	7948.87	1	7948.87	16.72	0.0015
AB	41.88	1	41.88	0.088	0.7717
AC	1925.41	1	1925.41	4.05	0.0671
AD	194.83	1	194.83	0.41	0.5341
BC	1563.37	1	1563.37	3.29	0.0948
BD	13.05	1	13.05	0.027	0.8712
CD	0.049	1	0.049	10230	0.9921
A^2	119.31	1	119.31	0.25	0.6254
B^2	2419.24	1	2419.24	5.09	0.0435
C^2	3720.14	1	3720.14	7.83	0.0161
D^2	237.37	1	237.37	0.50	0.4933
Residual	5703.66	12	475.30		
Lack of Fit	5123.01	10	512.30	1.76	0.4154
Pure Error	580.64	2	290.32		
Cor Total	307200	26			

Table 4 ANOVA table of thrust force (F_y) for Al_2O_3 nanofluid

Source	Sum of Squares	DF	Mean Square	F-value	Prob.
Model	55784.08	14	3984.58	29.74	< 0.0001
A-V	645.55	1	645.55	4.82	0.0486
B-f	13865.54	1	13865.54	103.48	< 0.0001
C-d	35279.87	1	35279.87	263.29	< 0.0001
D-np	716.73	1	716.73	5.35	0.0393
AB	114.76	1	114.76	0.86	0.3730
AC	1085.54	1	1085.54	8.10	0.0147
AD	1125.77	1	1125.77	8.40	0.0134
BC	19.67	1	19.67	0.15	0.7083
BD	2.06	1	2.06	0.015	0.9034
CD	64.44	1	64.44	0.48	0.5012
A^2	495.00	1	495.00	3.69	0.0787
B^2	223.68	1	223.68	1.67	0.2207
C^2	1349.45	1	1349.45	10.07	0.0080
D^2	2.86	1	2.86	0.021	0.8862
Residual	1607.96	12	134.00		
Lack of Fit	1517.95	10	151.79	3.37	0.2503
Pure Error	90.01	2	45.00		
Cor Total	57392.03	26			

Table 5 ANOVA table of feed force (F_x) for Al_2O_3 nanofluid

Source	Sum of Squares	DF	Mean Square	F-value	Prob.
Model	8713.82	14	622.42	68.48	< 0.0001

A-V	57.88	1	57.88	6.37	0.0267
B-f	2032.53	1	2032.53	223.63	< 0.0001
C-d	5944.62	1	5944.62	654.07	< 0.0001
D-np	169.74	1	169.74	18.68	0.0010
AB	3.77	1	3.77	0.41	0.5318
AC	56.79	1	56.79	6.25	0.0279
AD	52.82	1	52.82	5.81	0.0329
BC	45.97	1	45.97	5.06	0.0441
BD	0.42	1	0.42	0.046	0.8342
CD	2162	1	2162	23790	0.9879
A^2	17.36	1	17.36	1.91	0.1921
B^2	83.75	1	83.75	9.21	0.0104
C^2	136.78	1	136.78	15.05	0.0022
D^2	19.87	1	19.87	2.19	0.1650
Residual	109.06	12	9.09		
Lack of Fit	91.12	10	9.11	1.02	0.5930
Pure Error	17.95	2	8.97		
Cor Total	8822.89	26			

Table 6 ANOVA table of surface roughness (R_a) for Al_2O_3 nanofluid

Source	**Sum of Squares**	**DF**	**Mean Square**	**F-value**	**Prob.**
Model	4.04	14	0.29	19.21	< 0.0001
A-V	0.68	1	0.68	45.08	< 0.0001
B-f	2.67	1	2.67	177.47	< 0.0001
C-d	4681	1	4681	0.31	0.5870
D-np	0.34	1	0.34	22.79	0.0005
AB	0.012	1	0.012	0.79	0.3914
AC	0.011	1	0.011	0.73	0.4106
AD	44100	1	44100	0.029	0.8668
BC	302500	1	302500	2013	0.9650
BD	0.036	1	0.036	2.40	0.1471
CD	1406	1	1406	0.094	0.7649
A^2	0.017	1	0.017	1.10	0.3143
B^2	0.26	1	0.26	17.57	0.0012
C^2	5633	1	5633	0.37	0.5518
D^2	1365	1	1365	0.091	0.7682
Residual	0.18	12	0.015		
Lack of Fit	0.18	10	0.018	15.87	0.0607
Pure Error	2245	2	1122		
Cor Total	4.22	26			

The relationship between input variables and response parameters are modelled by quadratic regression. The regression models of cutting force (F_z), feed force (F_y), thrust force (F_x), and the surface roughness (R_a) with coefficient of determination (R^2) and adjusted R^2 equal to 98.14, 97.2, 98.76, 95.73, and 95.98, 93.93, 97.32, 90.75, respectively, are given below in Eq. 2-5.

$$F_z = -111.038 - 4.30154 * V + 3405.18 * f + 543.271 * d - 144.874 * np + 2.69646 * V * f + 2.43775 * V * d + 0.465267 * V * np + 1647.48 * f * d + 90.3 * f * np + 0.735 * d * np + 0.00525519 * V^2 - 13311.3 * f^2 - 293.452 * d^2 + 26.6852 * np^2$$

$$F_y = -27.0986 - 3.63287 * V + 2362.33 * f + 376.378 * d - 91.9392 * np - 4.46354 * V * f + 1.83042 * V * d + 1.11842 * V * np - 184.792 * f * d + 35.875 * f * np - 26.7583 * d * np + 0.0107044 * V^2 - 4047.53 * f^2 - 176.741 * d^2 - 2.93167 * np^2$$

$$F_x = 12.0813 - 1.08962 * V + 580.644 * f + 103.777 * d - 42.979 * np + 0.80875 * V * f + 0.418667 * V * d + 0.24225 * V * np + 282.5 * f * d + 16.125 * f * np + 0.155 * d * np + 0.00200486 * V^2 - 2476.72 * f^2 - 56.2681 * d^2 + 7.72 * np^2$$

$$R_a = 3.62992 - 0.00786944 * V - 21.2708 * f + 0.00458333 * d - 0.828333 * np - 0.0454167 * V * f - 0.00580556 * V * d - 0.0007 * V * np + 0.229167 * f * d + 4.75 * f * np - 0.125 * d * np + 0.0000619444 * V^2 + 139.062 * f^2 + 0.361111 * d^2 + 0.064 * np^2$$

In order to investigate the influence of nanoparticle concentration on various response variables, response surfaces are drawn in Fig 10. Figs 10(a-b) show that lowest cutting forces were recorded with the combination of highest nanoparticle concentration and lowest feed rate, and highest concentration and lowest depth of cut, respectively as reported by earlier researchers. Furthermore, Fig 10(c) shows the estimated responses surface for R_a in relation to nanoparticle concentration and cutting speed, while the feed and depth of cut are kept at middle level. The lowest surface roughness was achieved with a combination of highest nanoparticle concentration and highest cutting speed. It can be deduced from Fig 10(d) that lowest roughness was achieved with a combination of highest nanoparticle concentration and lowest feed rate.

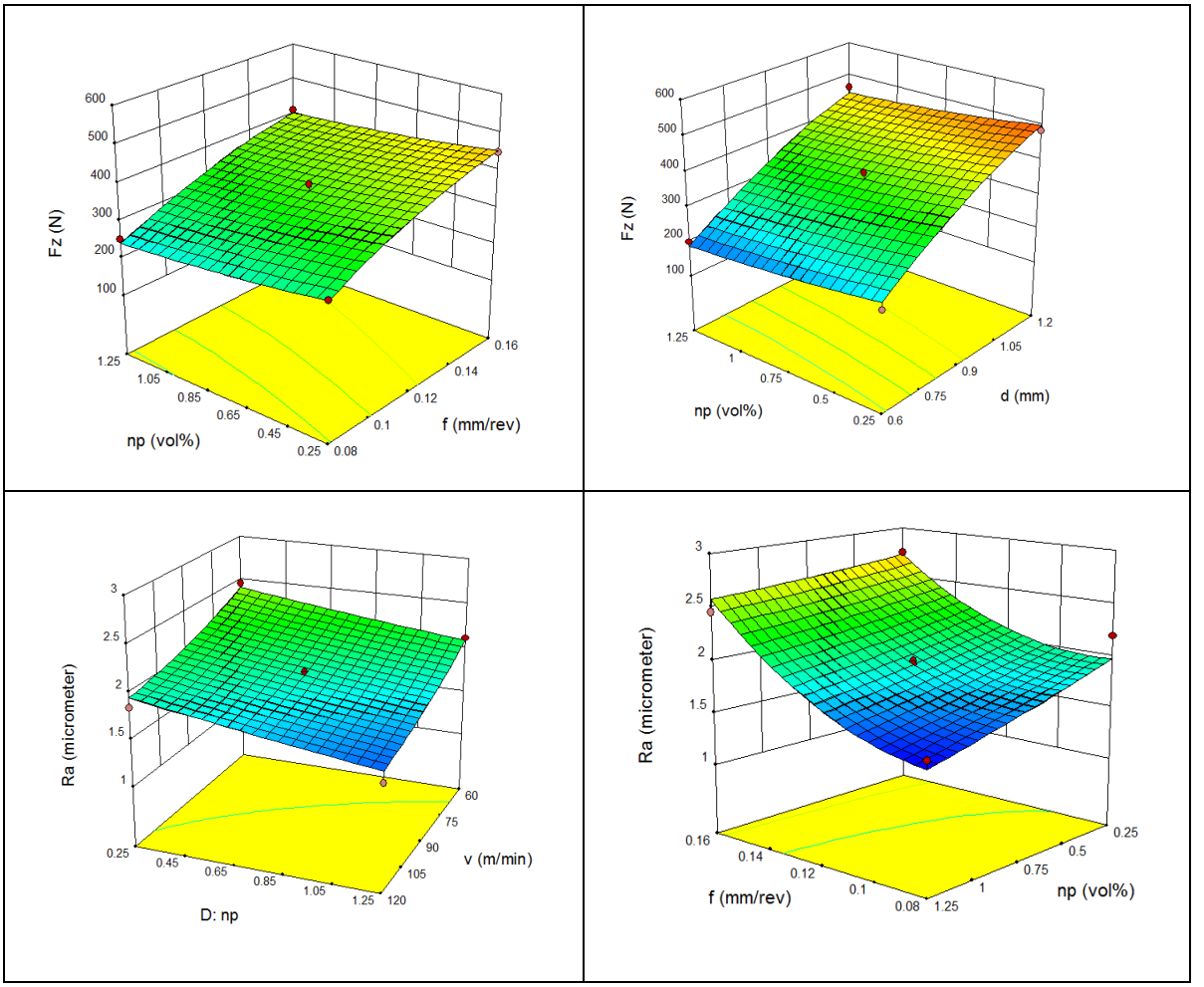

Fig. 10 Estimated response surface plots for Al_2O_3 nanoparticle concentration (np) versus v, f, and d

3.2 Machining with Alumina-graphene hybrid nanofluid

Tables 7-10 show the results of ANOVA, respectively for F_z, F_y, F_x, and R_a. This analysis was carried out at a confidence level of 95% (i.e. 5% significance level). The last column of these tables show the influence of variation in input variables (significant or non-significant) on response parameters (output). Table 7 show that np has a significant effect on cutting force. It can be seen from Tables 8-9 that np and its interaction with speed affect thrust and feed force significantly. In case of surface roughness, np has a significant effect but depth of cut does not affect roughness significantly as shown in Table 10. The findings are in the agreement with the results of investigations carried out by Dureja et al. (2009).

Table 7 ANOVA table of cutting force (F_z) for Al-GNP hybrid nanofluid

Source	Sum of Squares	DF	Mean Square	F-value	Prob.
Model	229400	14	16388.96	20.06	< 0.0001
A-V	3969.88	1	3969.88	4.86	0.0477
B-f	62473.46	1	62473.46	76.48	< 0.0001
C-d	128600	1	128600	157.45	< 0.0001
D-np	4930.83	1	4930.83	6.04	0.0302
AB	1806	1	1806	2211000	0.9988
AC	834.78	1	834.78	1.02	0.3320
AD	2460.53	1	2460.53	3.01	0.1082
BC	1631.21	1	1631.21	2.00	0.1830
BD	10.94	1	10.94	0.013	0.9098
CD	45.02	1	45.02	0.055	0.8184
A^2	191.37	1	191.37	0.23	0.6371
B^2	1738.62	1	1738.62	2.13	0.1703
C^2	8305.53	1	8305.53	10.17	0.0078
D^2	1212.63	1	1212.63	1.48	0.2465
Residual	9802.32	12	816.86		
Lack of Fit	9318.55	10	931.85	3.85	0.2236
Pure Error	483.77	2	241.89		
Cor Total	239200	26			

Table 8 ANOVA table of thrust force (F_y) for Al-GNP hybrid nanofluid

Source	Sum of Squares	DF	Mean Square	F-value	Prob.
Model	49291.60	14	3520.83	32.81	< 0.0001
A-V	538.12	1	538.12	5.01	0.0449
B-f	10274.65	1	10274.65	95.74	< 0.0001
C-d	28374.72	1	28374.72	264.40	< 0.0001
D-np	614.55	1	614.55	5.73	0.0339
AB	17.16	1	17.16	0.16	0.6963
AC	884.05	1	884.05	8.24	0.0141
AD	1922.32	1	1922.32	17.91	0.0012
BC	16.12	1	16.12	0.15	0.7051
BD	1.62	1	1.62	0.015	0.9043
CD	0.022	1	0.022	20940	0.9887
A^2	649.06	1	649.06	6.05	0.0301
B^2	673.91	1	673.91	6.28	0.0276
C^2	1445.24	1	1445.24	13.47	0.0032
D^2	142.05	1	142.05	1.32	0.2723
Residual	1287.81	12	107.32		
Lack of Fit	1214.61	10	121.46	3.32	0.2537
Pure Error	73.20	2	36.60		
Cor Total	50579.42	26			

Table 9 ANOVA table of feed force (F_x) for Al-GNP hybrid nanofluid

Source	Sum of Squares	DF	Mean Square	F-value	Prob.

Model	7025.91	14	501.85	32.58	< 0.0001
A-V	77.78	1	77.78	5.05	0.0442
B-f	1468.10	1	1468.10	95.32	< 0.0001
C-d	4039.54	1	4039.54	262.28	< 0.0001
D-np	87.41	1	87.41	5.68	0.0346
AB	2.10	1	2.10	0.14	0.7182
AC	125.89	1	125.89	8.17	0.0144
AD	273.74	1	273.74	17.77	0.0012
BC	2.30	1	2.30	0.15	0.7062
BD	0.23	1	0.23	0.015	0.9047
CD	1970	1	1970	12790	0.9912
A^2	93.27	1	93.27	6.06	0.0300
B^2	95.10	1	95.10	6.17	0.0287
C^2	206.67	1	206.67	13.42	0.0032
D^2	19.99	1	19.99	1.30	0.2768
Residual	184.82	12	15.40		
Lack of Fit	174.39	10	17.44	3.35	0.2519
Pure Error	10.42	2	5.21		
Cor Total	7210.73	26			

Table 10 ANOVA table of surface roughness (R_a) for Al-GNP hybrid nanofluid

Source	**Sum of Squares**	**DF**	**Mean Square**	**F-value**	**Prob.**
Model	2.50	14	0.18	16.84	< 0.0001
A-V	0.36	1	0.36	34.16	< 0.0001
B-f	1.33	1	1.33	125.68	< 0.0001
C-d	9607000	1	9607000	90750	0.9765
D-np	0.46	1	0.46	43.68	< 0.0001
AB	0.064	1	0.064	6.02	0.0304
AC	0.022	1	0.022	2.12	0.1715
AD	1.110E-003	1	1.110E-003	0.10	0.7516
BC	1.600E-005	1	1.600E-005	1.511E-003	0.9696
BD	2.662E-003	1	2.662E-003	0.25	0.6251
CD	0.027	1	0.027	2.56	0.1358
A^2	0.046	1	0.046	4.32	0.0598
B^2	0.16	1	0.16	15.31	0.0021
C^2	3.143E-003	1	3.143E-003	0.30	0.5958
D^2	3.185E-003	1	3.185E-003	0.30	0.5934
Residual	0.13	12	0.011		
Lack of Fit	0.13	10	0.013	17.22	0.0561
Pure Error	1.458E-003	2	7.291E-004		
Cor Total	2.62	26			

The regression models of cutting force (F_z), feed force (F_y), thrust force (F_x), and the surface roughness (R_a) with coefficient of determination (R^2) and adjusted R^2 equal to 95.91, 98.21, 96.81, 95.22, and 91.13, 96.13, 93.09, 89.63, respectively, are given below in Eq. (6-9).

$$F_z = -520.511 + 0.773165 * V + 2886.49 * f + 1153.88 * d - 269.327 * np + 0.0177083 * V * f - 1.60514 * V * d + 1.65346 * V * np + 1682.84 * f * d + 82.6875 * f * np - 26.6896 * d * np - 0.00653913 * V^2 - 11086.8 * f^2 - 457.037 * d^2 + 62.1807 * np^2$$

$$F_y = 4.87759 - 4.32011 * V + 2670.17 * f + 388.194 * d - 181.331 * np - 1.72594 * V * f + 1.65183 * V * d + 1.46147 * V * np - 167.281 * f * d + 31.8 * f * np - 0.596335 * d * np + 0.0120427 * V^2 - 6902.49 * f^2 - 190.651 * d^2 + 21.2823 * np^2$$

$$F_x = 2.46486 - 1.63901 * V + 1001.03 * f + 146.716 * d - 68.3962 * np - 0.604167 * V * f + 0.623333 * V * d + 0.5515 * V * np - 63.125 * f * d + 12 * f * np - 0.176543 * d * np + 0.00456523 * V^2 - 2592.99 * f^2 - 72.0949 * d^2 + 7.98364 * np^2$$

$$R_a = 1.71065 - 0.00304714 * V - 9.01806 * f + 0.709725 * d + 0.284886 * np - 0.105183 * V * f - 0.00831331 * V * d - 0.0011108 * V * np + 0.166667 * f * d + 1.28998 * f * np - 0.654347 * d * np + 0.0001011 * V^2 + 107.048 * f^2 + 0.281137 * d^2 - 0.100771 * np^2$$

In order to investigate the influence of nanoparticle concentration on various response variables, response surfaces are drawn in Fig 11. Fig 11(a) shows the estimated responses surface for cutting force in relation to nanoparticle concentration and feed rate, while the speed and depth of cut are kept at middle level. The lowest cutting force was recorded with a combination of highest nanoparticle concentration and lowest feed. It can be deduced from Fig 11(b) that lowest cutting force was recorded with a combination of highest nanoparticle concentration and lowest depth of cut. Figs 11(c-d) show that lowest roughness were recorded with the combination of highest nanoparticle concentration and highest speed, and highest concentration and lowest feed rate, respectively as reported by earlier researchers.

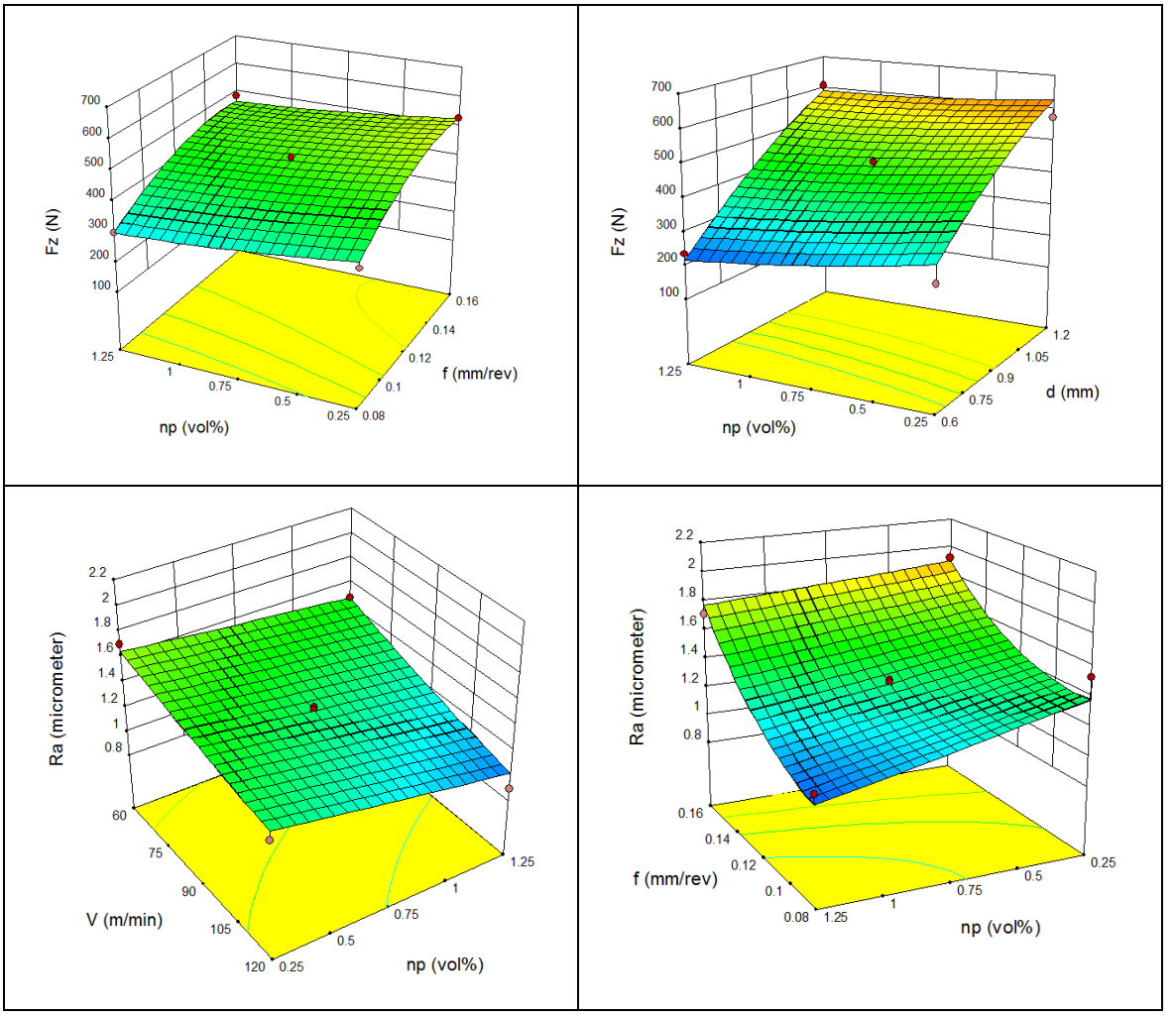

Fig 11 Estimated response surface plots for Al-GNP nanoparticle concentration (np) versus v, f and d

The values of response parameters (F_z, F_y, F_x, and R_a) recorded during the machining using different hybrid nanofluids are tabulated in Table 11. Results clearly reveal that Al-GnP hybrid nanofluid performed better compared to monotype alumina nanofluid. Use of Al-GnP hybrid nanofluid showed a significant reduction of 9.94%, 17.38%, 7.25%, and 20.28%, in F_z, F_y, F_x, and R_a, respectively over alumina nanoparticle mixed nanofluid.

Table 11 Performance comparison of different nanofluids

Nano-cutting fluid	**Cutting force (F_z)**	**Thrust force (F_y)**	**Feed force (F_x)**	**Roughness (R_a)**
Al_2O_3	138.09	108.55	38.02	1.430

Al_2O_3/ Graphene	124.36	89.68	35.26	1.140

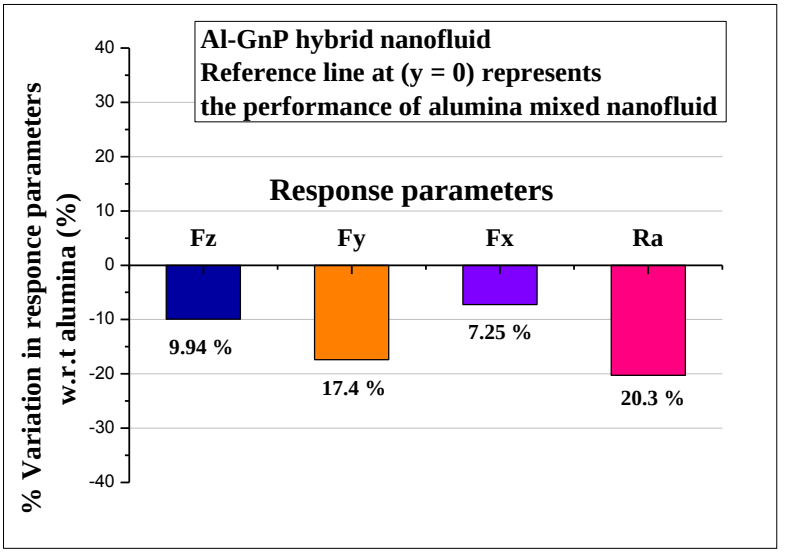

Fig 12 Effect of Al-GnP hybrid nanofluid on response parameters w.r.t. alumina nanofluid

3.3 Cutting forces

Table 11 shows that the lowest machining forces were recorded by using Al-GnP hybrid nanofluid. This may be because of the lowest coefficient of friction generated in the case of Al-GnP hybrid nanofluid as shown in Fig 5(c) which depicts that Al-GnP possesses the lowest coefficient of friction followed by alumina nanofluid. The lower value of the coefficient of friction reduced the friction force and hence the machining forces. Additionally, the viscosity of Al-GnP hybrid nanofluid is found to be higher compared to alumina nanofluid which helped in keeping the value of friction between the sliding surfaces at lower level and hence reduced the machining forces. Moreover, the nano-layer formed between the tool and chip surface might have reduced the direct contact and could prevent the damage of cutting tool.

3.4 Surface roughness

Table 11 illustrates that the lowest surface roughness was achieved by the use of Al-GnP hybrid nanofluid followed by alumina nanofluid. The probable reason may be the reduced coefficient of friction and formation of liquid-film of nanocutting fluid between the sliding surfaces. Moreover, the GnP nanoparticles mixed in base fluid enhanced the nanofluids wettability as shown in Fig 8.

The higher wettability of hybrid nanofluid enhances the effective spreading of cutting fluid at the machining zone and between the sliding surfaces. This might be helpful in two ways; firstly it might have reduced the friction coefficient at the tool-work piece interface during the machining because of the nano-ball bearing effects of nanoparticles present in nano-film. Secondly, due to the higher contact area available over the cutting tool, the nanofluid could have extracted more heat from the cutting tool compared to alumina nanofluid with lower wettability. Therefore, the temperature rise could remain under control which helped the tool to sustain its hardness and hence the sharpness of cutting edge. A noticeable difference in the quality of surfaces could be observed in Fig 6, which clearly illustrates that good quality surface is generated in the case of Al-GnP hybrid nanofluid and hence proves it to be the superior lubricant over alumina nanofluid.

4. Conclusions

Present study investigates the machining performance of hybrid nanofluid regarding the machining forces (F_z, F_y and F_x) and surface roughness (R_a). Al_2O_3 mixed nanofluid was hybridized with graphene nanoplatelets in a volumetric ratio of 90:10 to develop Al-GnP hybrid nanofluid. The optimization of different machining input variables (cutting velocity, feed rate, depth of cut and nanoparticle concentration) for response parameters using both Al_2O_3 and Al-GnP hybrid nanofluid with RSM technique was performed. Based on the results and discussion, the following conclusions could be drawn:

- The effective thermal conductivity of all studied nanofluids increases with an increase of temperature as well as particle volume fraction.
- Al-GnP hybrid and alumina nanofluids have shown an improvement in thermal conductivity over base fluid while surprisingly; the hybridization of alumina in graphene reduced its (hybrid nanofluid) thermal conductivity. An enhancement of 9.38% in thermal conductivity was recorded for Al-GnP hybrid, while alumina alone has shown an improvement of 9.85%, over base fluid.
- The effective viscosity of all the nanofluids is found to increase with an increase in the particle volume fraction and decrease with an increase in the temperature. The Al-GnP hybrid nanofluid exhibited higher viscosity than that of Al_2O_3 mixed nanofluid.
- Hybrid nanofluids has shown a remarkable improvement in machining performances over

Al_2O_3 mixed nanofluid. A significant reduction of 9.94%, 17.38%, 7.25%, and 20.28% in F_z, F_x, F_y, and R_a, respectively, could be achieved by using Al-GnP hybrid nanofluid over Al_2O_3 mixed nanofluid. Furthermore, with its use as a cutting fluid, the lowest values of 124.36 N, 89.68 N, 35.26 N, 1.140 µm, respectively, could be recorded for cutting force, thrust force, feed force, and surface roughness.

References

[1] Cetin, M.H., Ozcelik, B., Kuram, E., Demirbas, E., 2011. Evaluation of vegetable based cutting fluids with extreme pressure and cutting parameters in turning of AISI 304L by Taguchi method. J. Clean. Prod. 19, 2049-2056.

[2] Hadad, M., Sadeghi, B., 2013. Minimum quantity lubrication-MQL turning of AISI4140 steel alloy. J. Clean. Prod. 54, 332-343.

[3] Sharma, A.K.; Tiwari, A.K.; Dixit, A.R. 2016. Effects of minimum quantity lubrication (MQL) in machining processes using conventional and nanofluid based cutting fluids: A comprehensive review. Journal of Cleaner Production 127, 1-18.

[4] Sarıkaya, M., Güllü, A., 2015. Multi-response optimization of minimum quantity lubrication parameters using Taguchi-based grey relational analysis in turning of difficult-to-cut alloy Haynes 25. J. Clean. Prod. 91, 347e357.

[5] Tiwari, A.K.; Ghosh, P.; Sarkar, J. Investigation of thermal conductivity and viscosity of nanofluids. *Journal of Environmental Research and Development* **2012**, 7(2), 768-777.

[6] Yang, Y. Carbon nanofluids for lubricant application; PhD thesis: University of Kentucky**,** United States, 2006.

[7] Choi, S.U.S.; Zhang, Z.G.; Yu, W.; Lockwood, F.E.; Grulke, E.A. Anomalous thermal conductivity enhancement in nanotube suspensions. *Applied Physics Letters* **2001,** 79(14), 2252–2254.

[8] Sharma, A.K.; Tiwari, A.K.; Dixit, A.R. Progress of nanofluid application in machining: a Review. *Materials and Manufacturing Processes* **2015a**, 30(7), 813-828.

[9] Sharma, P., Sidhu, B.S., Sharma, J. 2015b. Investigation of effects of nanofluids on turning of AISI D2 steel using minimum quantity lubrication. J Clean. Prod. 108, 72-79.

[10] Lee, C.G.; Hwang, Y.J.; Choi, Y.M.; Lee, J.K.; Choi, C.; Oh, J.M. A Study on the

Tribological Characteristics of Graphite Nano Lubricants. *International Journal of Precision Engineering and Manufacturing* **2009**, 10(1), 85-90.

[11] Reddy, N.S.K.; Rao, P.V. Experimental investigation to study the effect of solid lubricants on cutting forces and surface quality in end milling. *International Journal of Machine Tools and Manufacture* **2006**, 46, 189-198.

[12] Khandekar, S.; Sankar, M.R.; Agnihotri, V.; Ramkumar, J. Nano-Cutting Fluid for Enhancement of Metal Cutting Performance. *Materials and Manufacturing Processes* **2012**, 27(9), 963-967.

[13] Park, K.H.; Ewald, B.; Kwon, P.Y. Effect of nano-enhanced lubricant in minimum quantity lubrication balling milling. Journal of Tribology 2011, 133=031803, 1–8.

[14] Alberts, M.; Kalaitzidou, K.; Melkote, S. An investigation of graphite nanoplatelets as lubricant in grinding. International Journal of Machine Tools and Manufacture 2009, 49, 966–970.

[15] Sayuti, M.; Sarhan, A.A.D.; Salem, F. Novel uses of SiO_2 nano-lubrication system in hard turning process of hardened steel AISI4140 for less tool wear, surface roughness and oil consumption. *Journal of Cleaner Production* **2014,** 67, 265-276.

[16] Amrita, M.; Srikant, R.R.; Sitaramaraju, A.V. Performance Evaluation of Nanographite-Based Cutting Fluid in Machining Process. *Materials and Manufacturing Processes* **2014**, 29, 600-605.

[17] Sarkar, J. & Ghosh, P., 2015. A review on hybrid nanofluids: Recent research, development and applications. *Renewable and Sustainable Energy Reviews*, 43, pp. 164-177.

[18] X. Zhang, C. Li, Y. Zhang, D. Jia, B. Li, Y. Wang, M. Yang, Y. Hou, X. Zhang, Performances of Al2O3/SiC hybrid nanofluids in minimum-quantity lubrication grinding, Int. J. Adv. Manuf. Technol. 1-15 (2016).

[19] Ahammed, N., Asirvatham, L. G. & Wongwises, S., 2016. Entropy generation analysis of graphene-alumina hybrid nanofluid in multiport minichannel heat exchanger coupled with thermoelectric. *International Journal of Heat and Mass Transfer*, *103*, pp. 1084-1097.

[20] Y. Zhang, C. Li, D. Jia, D. Zhang, X. Zhang, Experimental evaluation of the lubrication performance of MoS 2/CNT nanofluid for minimal quantity lubrication in Ni-based alloy grinding, Int. J. Mach. Tools Manuf. 99 (2015) 19–33.

[21] Abbasi, S. M., Rashidi, A., Nemati, A. & Arzani, K., 2013. The effect of Functionalization method on the stability and the thermal conductivity of nanofluid hybrids of carbon nanotubes/gamma alumina. *Ceramics International, 39*, pp. 3885-3891.

[22] Kanthavel, K., Sumesh, K., & Saravanakumar, P., 2016. Study of tribological properties on $Al/Al_2O_3/MoS_2$ hybrid composite processed by powder metallurgy. *Alexandria Engineering Journal, 55*, pp. 13-17.

[23] Young, T., 1805. An essay on the cohesion of fluids. *Philosophical Transactions of the Royal Society London*, 95, pp. 65-87.

[24] Wasan, D., Nikolov, A. & Kondiparty, K., 2011. The wetting and spreading of nanofluids on solids: Role of the structural disjoining pressure. *Current Opinion in Colloid & Interface Science* 16 (2011) 344-349.

[25] Montgomery, D.C., 2009. Design and Analysis of Experiments. Seventh ed. New York: John Wiley & Sons.

[26] Gopal, A.V. & Rao, P.V., 2003. Selection of Optimum Conditions for Maximum Material Removal Rate with Surface Finish and Damage as Constraints in SiC Grinding. *International Journal of Machine Tools & Manufacture*, 43, pp. 1327-1336.

[27] Bouacha, K., Yallese, M.A., Mabrouki, T. & Rigal, J.F., 2010. Statistical analysis of surface roughness and cutting forces using response surface methodology in hard turning of AISI 52100 bearing steel with CBN tool. *International Journal of Refractory Metals and Hard Materials*, 28, pp. 349-361.

[28] Dureja, J.S., Gupta, V.K. & Dogra, M., 2009. Design optimization of cutting conditions and analysis of their effect on tool wear and surface roughness during hard turning of AISI-H11 steel with a coated mixed ceramic tool. *Journal of Engineering Manufacture*, 223(B), pp. 1441-1453.